Supplementary Information **for Uno et al., Forward and inverse methods for extracting climate and diet information from stable isotope profiles in proboscidean molars**

Authors: Kevin T. Uno, Daniel C. Fisher, George Wittemyer, Iain Douglas-Hamilton, Nancy Carpenter, Patrick Omondi, Thure E. Cerling

1 Methods

1.1 Tusk preparation

Cutting of Misha's tusk in preparation for the analyses described below deserves brief mention here, as it varied slightly from the preparation of R37's tusk (Uno, 2012). The left tusk of Misha was selected for study because it was the longer of her tusks (96.2 cm). The tusk was transversely cut at the proximal end during the necropsy, and approximately 5 to 20 cm of the pulp cavity is missing from the proximal end. The tusk was cut longitudinally down the growth axis using a slow-speed (~220 feet per minute) band saw at the University of Michigan. A second longitudinal cut was made parallel to the first to isolate a 1 cm thick research slice. The research slice was then cut normal to the longitudinal cut but along the tusk axis to separate the upper and lower halves of the tusk. The upper half, termed the working half, was cut into nine 8 x 4 x 1 cm slabs, leaving the proximal end of the slab intact as a single 17 cm long piece. The lower half of the research slice, or archive half, was left entirely intact.

1.2 Micro-CT of molars

Micro-CT was used to determine 1) initial enamel density (f_i) as a function of final enamel density and 2) maturation length (l_m). These parameters are included in both the forward and inverse models. Two developing molars were selected for micro-CT analysis. Misha's lower right m3 (Misha_Rm3) consisted of four plates that were in the incipient stage of being joined together by cementum and a fifth loose plate (Misha_Rm3.5), which was chosen for micro-CT analysis. Photos taken during the

necropsy show two additional loci of pulp tissue posterior to the fifth plate (presumably related to what would have been a sixth and seventh plate), but they could not be identified with certainty during sample selection. The lower m1 (or m2) from K07-M53 consists of 9 plates, 5 of which were in early stages of being joined together by cementum and four additional loose plates. The posterior loose plate (K07-M53_m1.9) was chosen for micro-CT analysis. This is the most diminutive plate at 6.5 cm in length. Longitudinal sections measuring 5 mm in width were cut from near the center of each molar plate using a Buehler Isomet® slow speed saw. For Misha_Rm3.5, the section ran the full length of the tooth (~10 cm). Dentin was cut away in some places, but at least some dentin and the full thickness of enamel were present in the prepared section. The molar plate section was then cut into thirds, with each piece ranging from 3 to 4 cm in length. The molar section from K07-M53_m1.9 was cut from the lower ~3.8 cm of the plate.

Micro-CT scans were done near the top and bottom of the K07-M53_m1.9 section (Fig. 3B, main text), and at the top and bottom of each of the three pieces of the Misha_Rm3.5 molar section, for a total of eight scans. A piece of elephant tusk dentin and an isolated fragment of mature elephant molar enamel were also scanned to develop a calibration curve used to convert grayscale values to absolute densities. Densities of the enamel chip, tusk dentin fragment, and a marble of known density were determined using a pycnometer.

All scans were done on an Xradia® Micro XCT-400 at 60kV/10W and 4x magnification. The instrument and analytical method are described in detail in Hsieh (2012). Scan volumes were 5 mm^3 with resolution of 5.05 μm/voxel, resulting in ~1000 slices per scan. Unsigned 16-bit (U16) data files (~2GB) were reduced to unsigned 8-bit (U8) files (~1GB) using the software program MIPAV to facilitate data processing. During conversion from U16 to U8 files, the maximum U16 grayscale value was set at 255 on the U8 grayscale (0 to 255).

Stacks were analyzed in ImageJ (version 10.2) by taking a series of linear grayscale profiles normal to the EDJ using a 10 to 25 pixel-width line. Within each 5 mm^3 scan volume, profiles were taken in two to five slices across the entire thickness of the dentin and enamel. Profiles were smoothed with a 10-point running mean and converted from grayscale to percent of maximum enamel density based on the density calibration data.

1.3 Histological sample preparation and analysis

1.3.1 Molar thin sections and flatbed scans.

Thin sections were made from Misha molar plate Misha_Rm3.5, TE-95 m3 molar plate 7 (TE-95_Rm3.7), and the isolated enamel plate from the American Falls mammoth (IMNH-40368). Molar plates were cut longitudinally on a Buehler Isomet® slow speed saw to a thickness of several millimeters. Due to their length (~10 cm), plates were cut transversely into smaller pieces to fit onto oversized or standard petrographic slides. Misha_Rm3.5 was already cut into three pieces for micro-CT analysis (a, b, and c; Fig. S2), and TE-95_rm3.7 (Fig. S3) and IMNH-40368 (Fig. S4) were each cut into two pieces (a and b). When making transverse cuts, plates were partially cross-cut with the

Isomet saw, but the final portion of enamel to be in contact with the slide was broken by hand in an attempt to eliminate loss of material from saw blade kerf (~0.5 mm). Longitudinal sections were polished to 600 grit on a lap and epoxied to frosted oversized or standard petrographic slides. Molar plate thick sections were then cut to a thickness of ~500 μm, polished by hand on emery paper using successively finer grits from 600 to 2500 grit followed by 1.0- to 0.3- micron Buehler® aluminum oxide grit on a lap. Finished thicknesses ranged from 80 to 150 μm.

Photomicrographs of the three molar thin sections were taken using a Canon® Powershot SD750 digital camera coupled to a petrographic microscope with a custom-fabricated digital camera adapter. Images were taken at 25 to 400x magnification under transmitted plane-polarized light. Images were also taken at 25x magnification of the Misha_Rm3.5 thin section under crossed polars. A photomicrograph of a stage micrometer with 10-μm graduations was included with each sequence of thin section photomicrographs for scale. Magnification was selected so that the field of view of a photomicrograph captured the full enamel thickness in each image. Individual photomicrographs from the cervical margin to the apical end of the molar plates Misha_Rm3.5 (Fig. S2), TE-95_rm3.7 (Fig. S3), and IMNH-40368 (Fig. S4) were stitched together in Adobe® Photoshop to produce composite images of the enamel on the posterior side of each molar plate.

1.3.2 Tusk thin sections and flatbed scans.

One longitudinal surface of each ivory (tusk dentin) slab was polished in order to develop spatially accurate serial sampling plans for tusk dentin. Thin sections were made from the transverse surface of the proximal end of every other slab from the pulp cavity margin to the tip of the tusk to enable histological analysis for determining tusk growth rate. Methods for slab polishing, thin section preparation, and flatbed scans of polished longitudinal surfaces, and taking photomicrographs of thin sections are also described in Uno (2012).

A thin section was not prepared from slab M640, so instead, the transverse face was polished and scanned in color at 9600 dpi using an Epson® 4490 Photo flatbed scanner. The image was converted to gray scale and levels were adjusted in Photoshop to enhance growth increments for histological analysis (Fig. S5).

1.3.3 Histological analyses of tusk and molars.

ImageJ was used for histological analysis of enamel thin sections and flatbed scans of tusk dentin slab M640. Second-order growth increments in M640 were measured in ImageJ. The base of slab M640 was cut along the tusk axis, and therefore, the angle θ between the tusk axis and the growth increments on the longitudinal surface was measured in multiple places to compare axial ^{14}C- and radial increment-based growth rates (Fig. S5).

Crown formation time (CFT) in proboscidean teeth was measured using histological features observed in thin section following the method of Dirks et al. (2012). To determine CFT, the appositional angle α must be measured, where α is defined as the

angle between striae of Retzius and the EDJ. The daily secretion rate (DSR) must also be measured. DSR is the thickness of enamel secreted daily by ameloblast cells along enamel prisms. Given α and DSR, one can use trigonometry to calculate daily extension rate (DER), which represents the daily length of crown extension from the apical end to the cervix. The angle α was measured from Misha, TE-95, and IMNH-40368 thin sections (Figs S2, S3, and S4, respectively) and DSR was measured or estimated to calculate CFT.

1.4 Sampling tusks and molars for isotope analysis

1.4.1 Tusk dentin sampling and pretreatment.

Tusk dentin slab M640 was selected for sampling based on ^{14}C-derived growth rates that indicate the dentin in M640 captures the move from California to Utah. 175 samples were end-milled from tusk dentin slab M640 at 100 to 200 μm resolution (Uno, 2012). End-milling is a common milling technique whereby a drill bit with cutting teeth on the end and the sides of the bit is used to contour-cut along a surface. In this case, we end-milled along contour paths defined incremental growth features in the polished tusk dentin. Contour paths were done on a computer-controlled micro milling machine (Merchanteck Micromilll). Once a series of drill paths were drawn, the end-mill bit (Brasseler, # H21.11.010) plunged into the tusk slab a depth of 1mm. Next, the slab was contour-milled at 100 to 200 μm width sampling resolution, which corresponds to approximately one and two week's time, respectively. The bit travelled along the contoured path at 20 μm/sec. Dentin powder was collected between each successive end milling pass. A flatbed scan of slab M640 after micromilling is shown in Fig. S5. The tusk profiles serve as the primary $\delta^{13}C$ and $\delta^{18}O$ input signals.

Tusk profile data from dentin slab R37-DEN-412 (n=239) are also used in this study as a primary input signal for molar plate R37_Rm3.8 (Uno, 2012). This slab was selected because based on bomb-curve ^{14}C growth rates, the tusk dentin in it formed over the same time interval as the posterior section of the R37 left m3. All serially sampled tusk dentin powders were reacted with a 30 % hydrogen peroxide solution in 0.65 ml centrifuge tubes for 30 minutes, rinsed with DI water and centrifuged three times, and then dried overnight at 60° C. Pretreatment resulted in a loss of *ca.* 40 % of initial sample mass.

1.4.2 Molar enamel sampling.

All molar plates sampled for intratooth profiles were sampled using the conventional drilling method. Each tooth was measured along the outer enamel surface of the plate from the cervix to the apical end and marked every centimeter with a pencil. After the first series of marks were made, a second set of marks was added every 2 mm. Using a Dremel tool with a 1 mm diameter carbide steel bit (Brasseler # H21.11.010), samples were drilled every ~2 mm from the outer enamel surface to a depth ranging from 0.5 to 1.2 mm deep for the Misha (Fig. S7), R37 (Fig. S8), and LACM molars. Sampling depth for the isolated enamel plate IMNH-40368 ranged from ~1.5 to ~3 mm, the latter of

which represents the full thickness of the enamel. After drilling, samples were scanned on a flatbed scanner and the sample lengths (Δx) and depths (Δz) were measured in ImageJ for accurate values to input into the inverse model.

Serially sampled enamel samples were reacted with a 3 % hydrogen peroxide solution in 1.7 ml centrifuge tubes for 30 minutes, rinsed with DI water and centrifuged three times; reacted with a 0.1 M Na-buffered acetic acid solution for 30 minutes, rinsed with DI water and centrifuged three times; and then dried overnight at 60° C.

Two other serial sampling methods were applied to sample Misha_Rm3.5b to generate intratooth profiles that captured isotopic shifts in $\delta^{13}C$ and $\delta^{18}O$ associated with the move from CA to UT. The two additional profiles allow comparison of high-resolution sampling methods with the m_{est} generated by running conventionally sampled profile data in the inverse model.

The first high-resolution sampling method was micromilling 50 μm thick enamel samples parallel to the appositional surface using an end-milling technique for tusk dentin (Uno, 2012). The appositional angle, α, was measured in multiple places along the EDJ on the thin section. Scan lines were then mapped onto the molar sample using the micromill software, and 36 samples were end-milled from the outer enamel surface to the EDJ (Fig. S9). The outermost nine paths were milled at 100 μm thickness to produce enough powder for analyses because of shorter effective path lengths. All sample powders generated by conventional and micromilling methods were analyzed without pretreatment. Samples from immature portions of enamel likely still contained organics associated with the secretory phase of enamel formation.

The second high-resolution sampling technique is laser ablation gas chromatography IRMS (LA-GC-IRMS). Thermal ablation of enamel using a CO_2 laser has been primarily used on rodent teeth. The method is minimally invasive as a single laser pit is ~250 μm in diameter and 100 μm depth (Passey and Cerling, 2006). Three profiles, each consisting of 13 or 14 scans, were done across the entire enamel thickness (2.8 to 3.0 mm) from the EDJ to the outer enamel surface. Profiles were done 54, 71, and 80 mm above the cervical margin (Fig. S10). Each scan consisted of CO_2 cryogenically pooled from five laser shots (8.5 milliseconds at 7.5 Watts) taken along a path parallel to the EDJ.

1.5 Stable carbon and oxygen isotope analysis

The carbonate component of hydroxylapatite in powdered tusk dentin and molar enamel samples was analyzed for stable carbon and oxygen isotope ratios, reported as δ-values relative to the Vienna Pee Dee Belemnite (VPDB) using permil (‰) notation where

$$\delta^{13}C\ (\delta^{18}O) = (R_{sample}/\ R_{standard} - 1) \times 1000 \qquad (1)$$

and R_{sample} and $R_{standard}$ are the $^{13}C/^{12}C$ ($^{18}O/^{16}O$) ratios in the sample and in the standard, respectively, and the $\delta^{13}C$ ($\delta^{18}O$) value of VPDB is defined as 0‰. Sample powders were digested in 100 % H_3PO_4 (phosphoric acid) using a Finnigan CarboFlo coupled to the dual inlet on a Finnigan MAT 252 IRMS at the University of Utah's Stable Isotope Ratio Facility for Environmental Research (SIRFER).

The CarboFlo system is a hybrid positive pressure/vacuum system with a common acid bath (CAB). Approximately 800 to 1000 μg of dentin (350 to 600 μg of enamel) was weighed out into a silver capsule, which was used as a precautionary measure to oxidize any SO_2 produced during digestion in phosphoric acid. Silver capsules containing powdered samples were dropped from an autosampler carousel into the vigorously stirred CAB and reacted for 10 (enamel) to 20 minutes (dentin) at 90 ± 2° C. A microcapillary tube submersed in the acid bath flushed it with 20 ml/minute of He and a 40 ml/minute He stream flushed the autosampler. The combined He streams swept the liberated H_2O and CO_2 through a dry ice/ethanol trap to remove water and then through a liquid nitrogen (LN) trap to collect the CO_2. Following the reaction period, the LN trap was isolated from positive pressure and evacuated with a rotary vacuum pump to ~10^{-3} Torr. The LN trap was removed and the CO_2 was cryogenically transferred to a microvolume held at -170°C. Once transferred to the microvolume, the CO_2 was analyzed through the dual inlet system on the IRMS. Internal laboratory standards of tusk dentin (R37-DEN), modern enamel (MCM, MRS), and calcite (UU Carrara) were used for data correction of samples and had average standard deviations of ~0.1 ‰ for $\delta^{13}C$ and ~0.2 ‰ for $\delta^{18}O$ across all analytical runs.

CO_2 liberated from enamel by LA-GC-IRMS was inlet via GC interfaced to a Finnigan MAT 252 IRMS in continuous flow. A correction of + 0.7 ‰ was applied to $\delta^{13}C$ laser values based on the average offset between laser and conventional $\delta^{13}C$ values from the portion of the molar that formed exclusively in Utah. A correction of + 7.4 ‰ was applied to $\delta^{18}O$ laser values. The + 7.4 ‰ offset is a result of liberating phosphate-bound oxygen, which is 8 to 9 ‰ enriched in ^{18}O compared to carbonate. Passey and Cerling (2006) report similar offsets of + 0.3 ± 1.1 ‰ for $\delta^{13}C$ and + 6.4 ± 0.7 ‰ for $\delta^{18}O$ in modern enamel.

1.6 Determination of body water turnover from tusk dentin isotopic data

We calculated the turnover time of body water in the zoo elephant, Misha, using the high-resolution oxygen isotope profile in the tusk dentin around the time of the move from California to Utah, where she arrived on April 22, 2005. Because there is some natural variabilty in the oxygen isotope ratio in the tusk dentin before and after the move, we take the mean $\delta^{18}O$ value over the month prior to the move ($\delta_{init} = -9.2$), where values are stable, and again during a priod of stability of approximately two months after the move ($\delta_{eq} = -13.9$) when they have reached the new equilibrium. Using the mean $\delta^{18}O$ values before and after the move, we calculate the half life ($t_{1/2}$) using the equation from Green et al. (2018b) and Podlesak et al. (2008) :

$$t_{1/2} = \frac{t \times \ln(2)}{\ln\left(\frac{\delta_{init} - \delta_{eq}}{\delta_t - \delta_{eq}}\right)} \quad (2)$$

The term δ_t is the $\delta^{18}O$ value at time t (in days) during the change. We solve for $t_{1/2}$ at six points that range from ~6 to 53 days after the water shift associated with the move and calculate the mean $t_{1/2}$ value.

1.7 Forward and inverse models

1.7.1 Forward model

We apply the forward model developed by Passey and Cerling (2002) to describe the effects of tooth enamel mineralization on $\delta^{13}C$ and $\delta^{18}O$ values. The three principal equations of the forward model that describe time averaging of the isotopic signal based on enamel maturation and sampling geometry are reviewed here. The first equation describes the isotopic composition of enamel in a volume parallel to the appositional surface *i* (see Figure 1 in main text) based on the mineralization parameters:

$$\delta_{ei} = (f_i * \delta_{mi}) + (1 - f_i) * \frac{\sum_{n=i+1}^{i+1+l_m} \delta_{m_n}}{l_m} \quad (3)$$

where δ_{ei} is the isotope ratio of the fully mineralized enamel, f_i is the initial density of the enamel as a fraction of the fully mineralized enamel, δ_{mi} is the isotope ratio of the input signal (diet or body water) during the secretory phase, and l_m is the maturation length (Figure 1). The model accounts for different sampling depths by casting the drilling depth as a function of l_a, where

$$\delta_{ci} = \frac{1}{l_a} \sum_{n=i-l_a}^{i} \delta_{e_n} \quad (4)$$

and δ_{ci} is the isotope ratio of the column of enamel drilled normal to the enamel surface and δ_{en} is the isotope ratio of each volume of enamel *i* deposited along the appositional surface through time (Figure 1). If the drilling depth is half or one-third of the way through the entire enamel thickness, then l_a in the first term of equation 3 is $0.5*l_a$, or $1/3*l_a$, respectively.

Finally, to account for the distance between samples along the growth axis of the tooth, the term sampling length (l_s) is introduced, which represents the distance between samples. If the sampling path is only 1 mm wide (parallel to the growth axis), but the distance between each sample path is 5 mm, then l_s is 5 mm. The isotope ratio of that portion of the enamel is modeled by averaging the number of columns in a sampling path such that

$$\delta_{di} = \frac{1}{l_s} \sum_{n=i-\frac{1}{2}l_s}^{i-1+\frac{1}{2}l_s} \delta_{c_n} \quad (5)$$

where δ_{di} is the isotope ratio over the sampling interval l_s.

1.7.2 Inverse model

In the inverse model developed by Passey et al. (2005), measured profile data **d** are related to the primary input signal **m** by the linear system

$$\mathbf{Am=d} \quad (6)$$

where **A** is an averaging matrix of dimensions *M x N*. The system of equations is under-determined because there are more unknown parameters *M* than measured data *N* and thus is considered an ill-posed problem. Menke (1989) and Zhdanov (2002) both provide an excellent background on discrete inverse theory from a geophysical perspective, and Passey et al. (2005) provide a more detailed description of the model, including code for running the inversion (mSolve1_1) and error measurement (Emeas1_1) in Matlab (version 7.10; R2010a).

Input parameters include f_i, l_a, l_m, sample length along the growth axis (Δx, or l_s in the forward model), and sample depth (Δz). These *a priori* inputs constrain the system, which is solved by determining a minimum length solution by the following equation:

$$\mathbf{m_{est}} = \langle \mathbf{m} \rangle + \mathbf{A^T}[\mathbf{AA^T} + \varepsilon^2\mathbf{I}]^{-1}[\mathbf{d} - \mathbf{A}\langle \mathbf{m} \rangle] \quad (7)$$

where m_{est} is the estimated primary input signal, $\langle \mathbf{m} \rangle$ is an *a priori M* x 1 reference vector, and the term $\varepsilon^2\mathbf{I}$ is a regularization parameter, where ε is the damping factor and **I** is an *N x N* identity matrix.

Primary constraints to the family of solutions generated by equation 6 are the regularization parameter, which is controlled by the damping factor (ε); the input parameters (and associated uncertainties); and a reference vector, which is constrained by the ecological range of $\delta^{13}C$ values or the $\delta^{18}O$ values of body water measured from an intratooth profile. An appropriate ε is essential for constraining the family of solutions to those that are realistic for the system. Smaller ε values return a longer (or more oscillatory) solution than larger ε values. To determine the appropriate ε, the model utilizes the Morozov discrepancy principle, whereby the predicted error (E_{pred}) calculated from ε is compared to the measured error (E_{meas}). E_{meas} is calculated (using the code in Emeas1_1) based on uncertainties in measured isotopic profile data, Δx, and Δz. These three variables are called r1, r2, and r3 in the model code and in main text Figures 11-14. An appropriate ε value returns an E_{pred} that is similar to the E_{meas} (Passey et al., 2005). Additional sensitivity tests used to evaluate inverse model results include changing the parameters f_i, l_a, l_m, as well as the reference vector range, value, and standard deviation (Fig. S15).

2 List of Supplementary Tables

Table S1. Measurements of second-order growth increment thickness (microns) in tusk dentin slab M640.

Table S2. Measurements of angle (θ) between tusk axis and growth increments and calculated radial growth rate in μm/week from tusk dentin slab M640

Table S3. Measurements of angle of apposition (a) from molar thin sections

Table S4. Measurements of enamel thickness in elephant molars

Table S5. Stable carbon and oxygen isotope profile data from M640 tusk dentin

Table S6. Conventionally sampled enamel stable isotope profile data from Misha_Rm3.5, R37_Rm3.8, LACM-47129, and IMNH-40368

Table S7. Micromill stable isotope profile data from Misha Rm3.5b enamel

Table S8. LA-GC-IRMS stable isotope profile data from Misha Rm3.5b enamel

3 References

Dirks, W., Bromage, T.G., Agenbroad, L.D., 2012. The duration and rate of molar plate formation in *Palaeoloxodon cypriotes* and *Mammuthus columbi* from dental histology. Quaternary International 255, 79-85.

Green, D.R., Olack, G., Colman, A.S., 2018. Determinants of blood water δ18O variation in a population of experimental sheep: Implications for paleoclimate reconstruction. Chemical geology 485, 32-43.

Hsieh, C.H., 2012. Procedure and analysis of mineral samples using high resolution x-ray micro tomography, Metallurgical Engineering. University of Utah, Salt Lake City, UT, p. 151.

Ingram, L.B., Weber, P.K., 1999. Salmon origin in California's Sacramento–San Joaquin river system as determined by otolith strontium isotopic composition. Geology 27, 851-854.

Jochum, K.P., Scholz, D., Stoll, B., Weis, U., Wilson, S.A., Yang, Q., Schwalb, A., Börner, N., Jacob, D.E., Andreae, M.O., 2012. Accurate trace element analysis of speleothems and biogenic calcium carbonates by LA-ICP-MS. Chemical Geology.

Menke, W., 1989. Geophysical data analysis: discrete inverse theory. Academic Press, San Diego.

Miller, W.E., 1971. Pleistocene vertebrates of the Los Angeles Basin and vicinity (exclusive of Rancho La Brea). Bulletin of the Los Angeles County Museum of Natural History Science: 10, 124.

Passey, B.H., Cerling, T.E., 2002. Tooth enamel mineralization in ungulates; implications for recovering a primary isotopic time-series. Geochimica et Cosmochimica Acta 66, 3225-3234.

Passey, B.H., Cerling, T.E., 2006. In situ stable isotope analysis ($d^{13}C$,$d^{18}O$) of very small teeth using laser ablation GC/IRMS. Chemical Geology 235, 238-249.

Passey, B.H., Cerling, T.E., Schuster, G.T., Robinson, T.F., Roeder, B.L., Krueger, S.K., 2005. Inverse methods for estimating primary input signals from time-averaged isotope profiles. Geochimica et Cosmochimica Acta 69, 4101-4116.

Pinsof, J.D., 1992. The late Pleistocene vertebrate fauna from the American Falls area, southeastern Idaho. Idaho State University.

Podlesak, D.W., Torregrossa, A.-M., Ehleringer, J.R., Dearing, M.D., Passey, B.H., Cerling, T.E., 2008. Turnover of oxygen and hydrogen isotopes in the body water, CO_2, hair, and enamel of a small mammal. Geochimica et Cosmochimica Acta 72, 19-35.

Scott, W., Pierce, K., Bradbury, J.P., Forester, R., 1982. Revised Quaternary stratigraphy and chronology in the American Falls area, southeastern Idaho. Cenozoic Geology of Idaho: Idaho Bureau of Mines and Geology Bulletin 26, 581-595.

Uno, K.T., 2012. Advances in terrestrial paleoecology from intratooth stable isotope profiles in tooth enamel and tusk dentin, Geology and Geophysics. University of Utah, Salt Lake City, UT, p. 307.

Uno, K.T., Quade, J., Fisher, D.C., Wittemyer, G., Douglas-Hamilton, I., Andanje, S., Omondi, P., Litoroh, M., Cerling, T.E., 2013. Bomb-curve radiocarbon measurement of recent biologic tissues and applications to wildlife forensics and stable isotope (paleo) ecology. Proceedings of the National Academy of Sciences 110, 11736-11741.

Zhdanov, M.S., 2002. Geophysical inverse theory and regularization problems. Elsevier Science Ltd, Netherlands.

4 Supplementary Figures (S1 to S16)

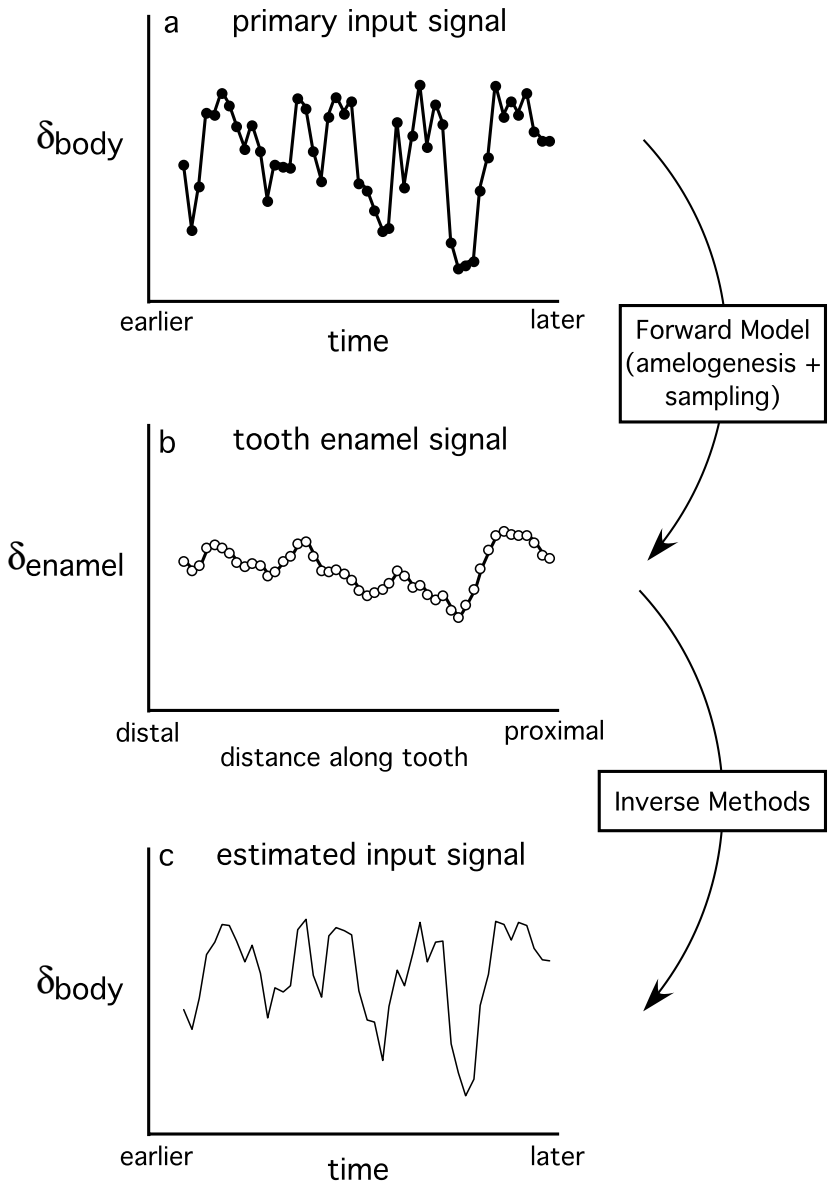

Figure S1. Schematic representation of forward and inverse models. From Passey et al., 2005.

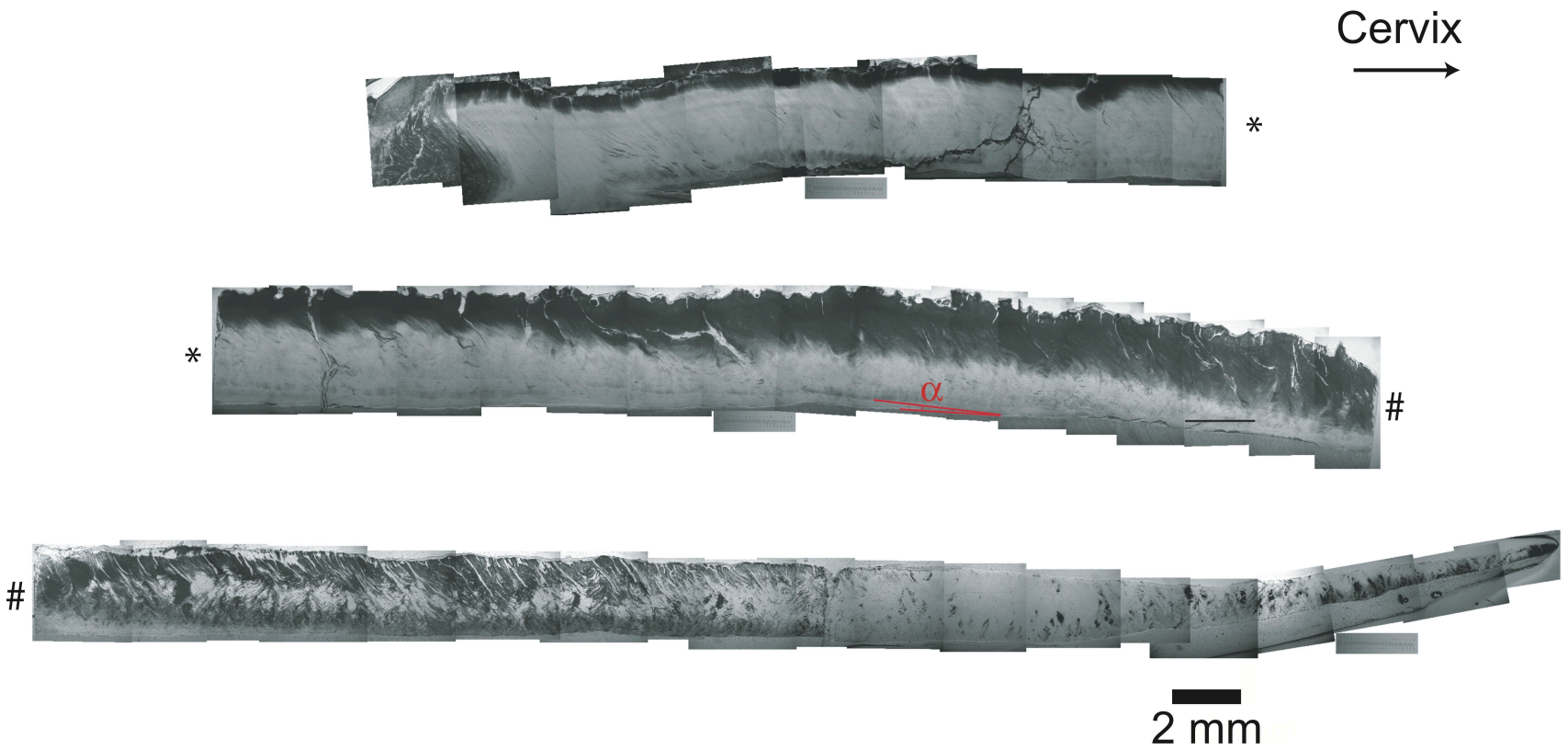

Figure S2. Composite photomicrograph from elephant molar thin section Misha_Rm3.5 at 40x magnification. The upper, middle, and lower images represent the top, middle, and bottom of the posterior side of the molar plate from the apical end to the cervix, which is toward the right in all three images. Image tie points are indicated by symbols (*,#). The entire enamel thickness is shown throughout most of the images, and the EDJ is at the base of each image.

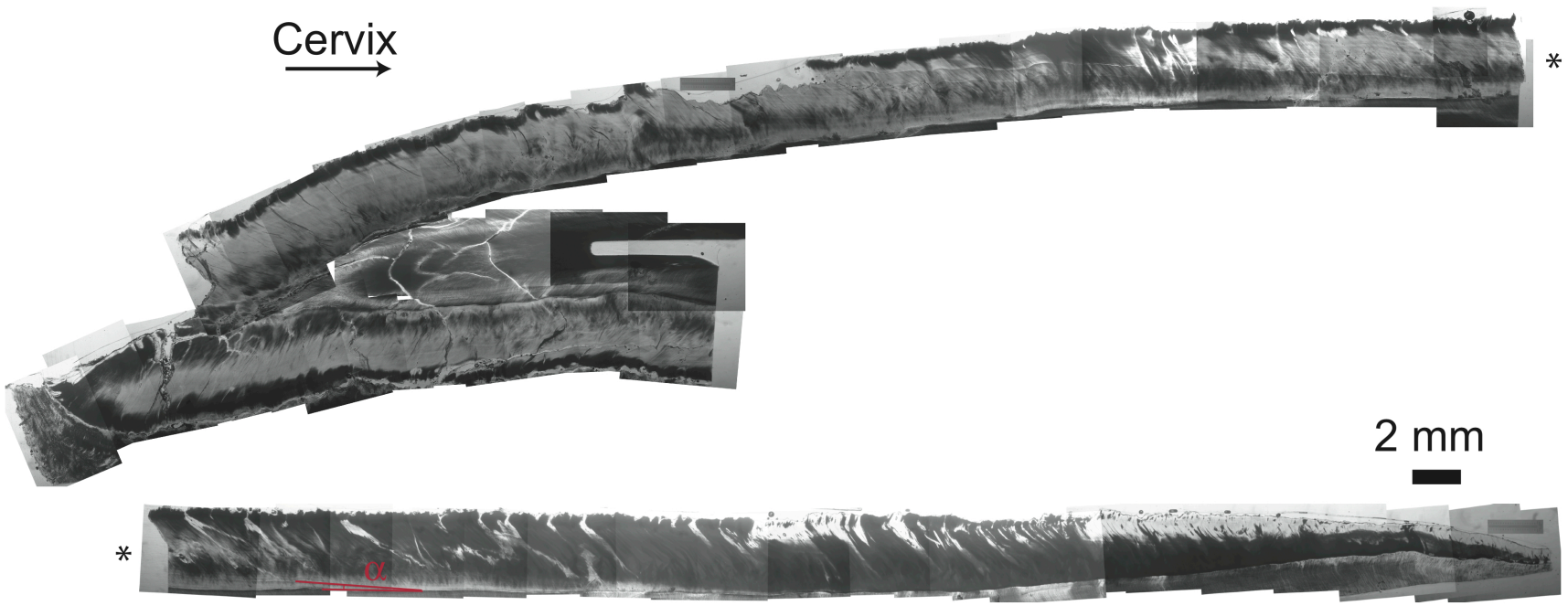

Figure S3. Composite photomicrograph from elephant molar thin section TE-95_Rm3.7 at 25x magnification. The upper and lower images comprise the posterior side of the molar plate from the apical end to the cervix, which is toward the right in both images. Image tie points are indicated by asterisks. The entire enamel thickness (~3 mm) is shown throughout most of the images, and the EDJ is at the base of each image.

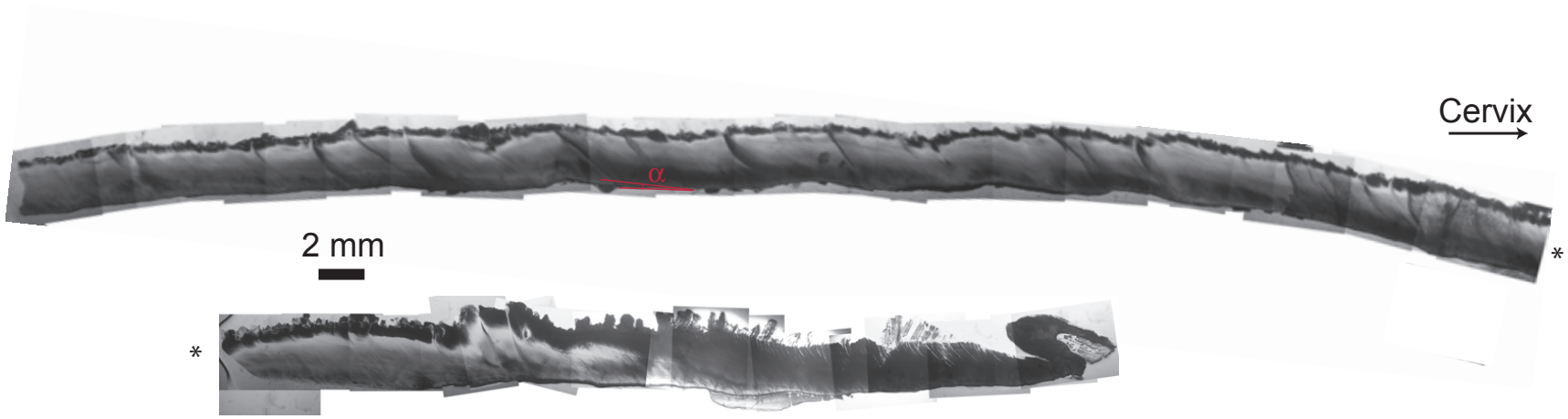

Figure S4. Composite photomicrograph from mammoth molar thin section IMNH-40368 at 25x magnification. The upper and lower images comprise the posterior side of the molar plate from the apical end to the cervix, which is toward the right in both images. Image tie points are indicated by asterisks. The entire enamel thickness (~2.8 mm) is shown throughout all images, and the EDJ is at the base of each image.

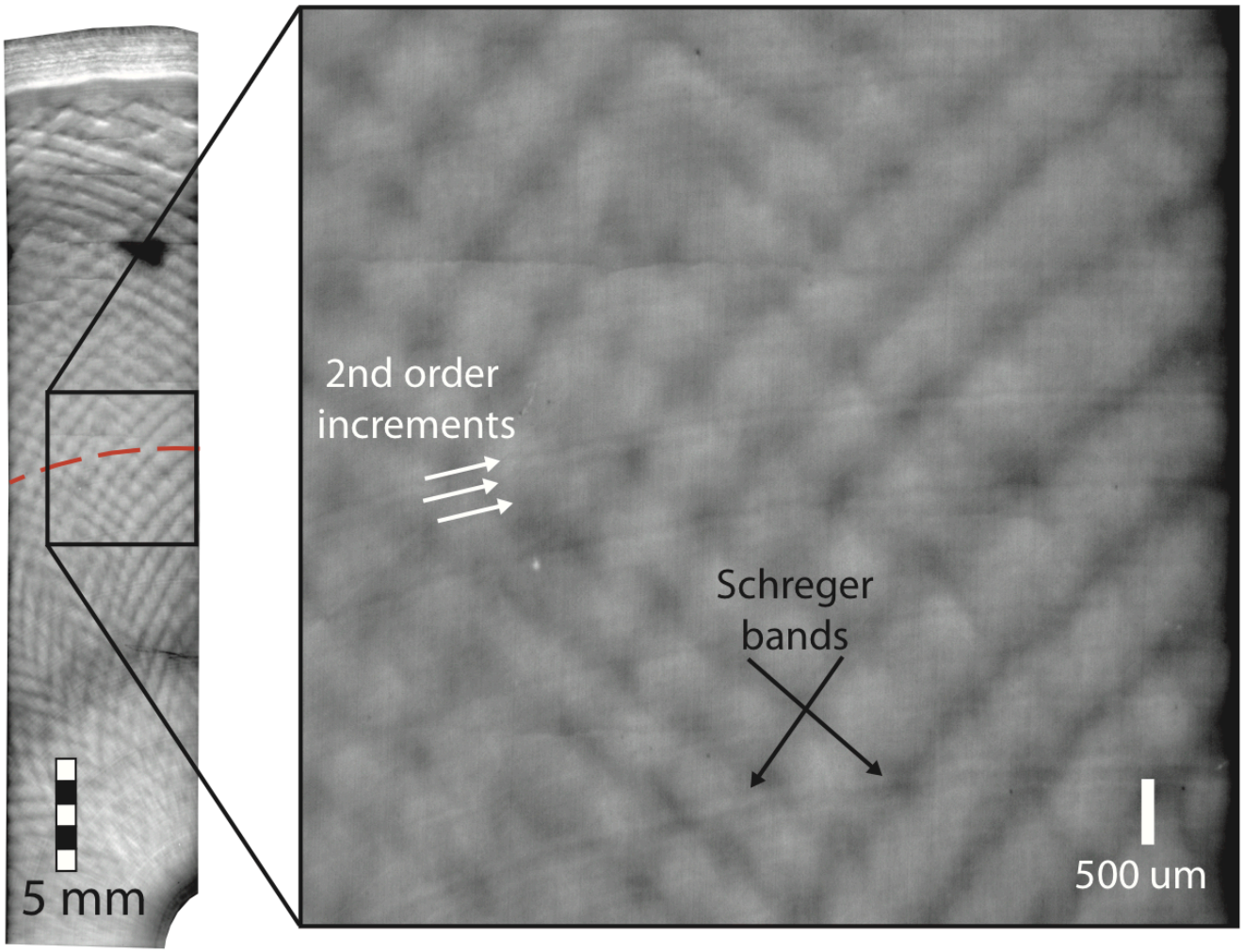

Figure S5. Flatbed scan of the proximal transverse side of Misha tusk dentin slab M640. The tip of the pulp cavity is shown in the lower right corner of the full scan (at left). A red dashed line marks the position where the isotopic shift associated with the move from CA to UT occurs. Scale bar is 5 mm in length. Inset (at right) illustrates selected second-order growth increment boundaries, each representing approximately one week, indicated by white arrows. Increment thicknesses were measured to determine radial growth rate.

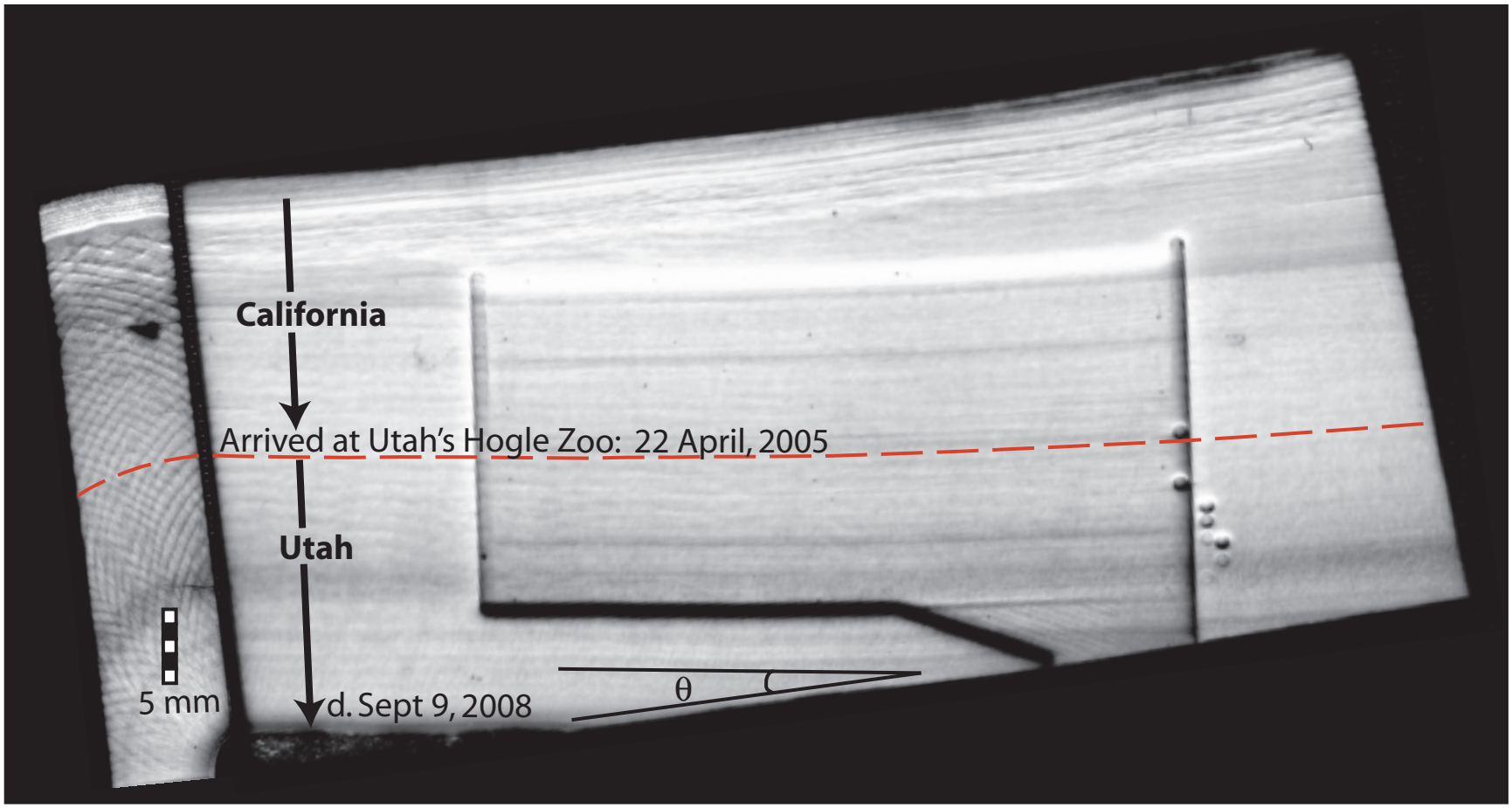

Figure S6. Flatbed scan of micromilled sample M640, with the proximal end to the left. On the left of the image is a transversely-cut piece reflected 90° about the vertical axis to show the tree-ring like structure. To the right is the polished longitudinally-cut slab after micromilling. The tip of the pulp cavity can be seen in the lower left part of the image. The red line is an isochron indicating the location of the isotopic shift associated with the move from CA to UT. The angle θ was measured at multiple places along the base of the slab to convert axial growth rate (or extension rate) to radial growth rate (or apposition rate), which enables comparison of axial ^{14}C-derived and radial histologically-derived growth rates.

Figure S7. Flatbed scan of conventionally drilled sample Misha_Rm3.5. Samples were drilled on the posterior side of the plate at intervals of 5 mm from 0 to 30 mm from the cervix and ~2 mm from 30 mm to the apical end of the tooth (~103mm).

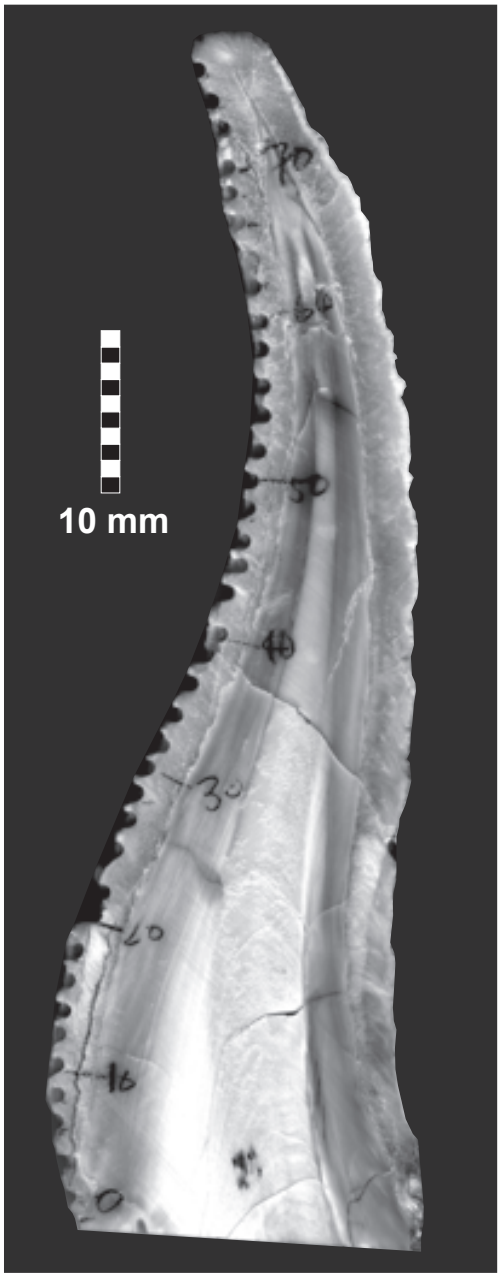

Figure S8. Flatbed scan of conventionally drilled molar plate R37_Rm3.8. Samples were drilled at ~2 mm intervals.

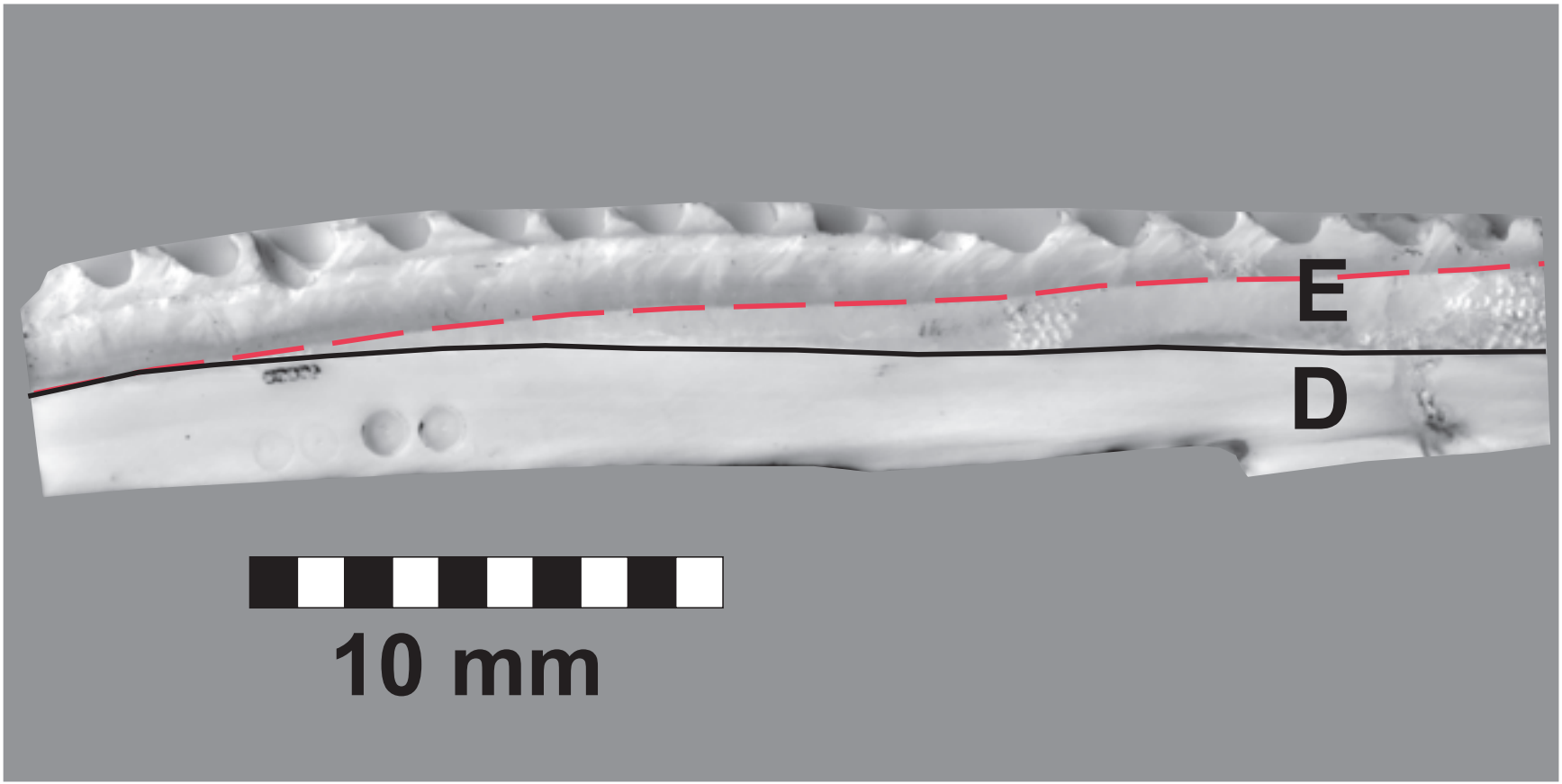

Figure S9. Image of sample Misha_Rm3.5b after micromill, laser, and conventional sampling. The black line marks the EDJ and the red dashed line marks the last micromilled scan. The angle of the micromill scans is approximately parallel to the appositional surface (red dashed line), which is ~3.2° offset from EDJ. Width of scale bar is 10 mm.

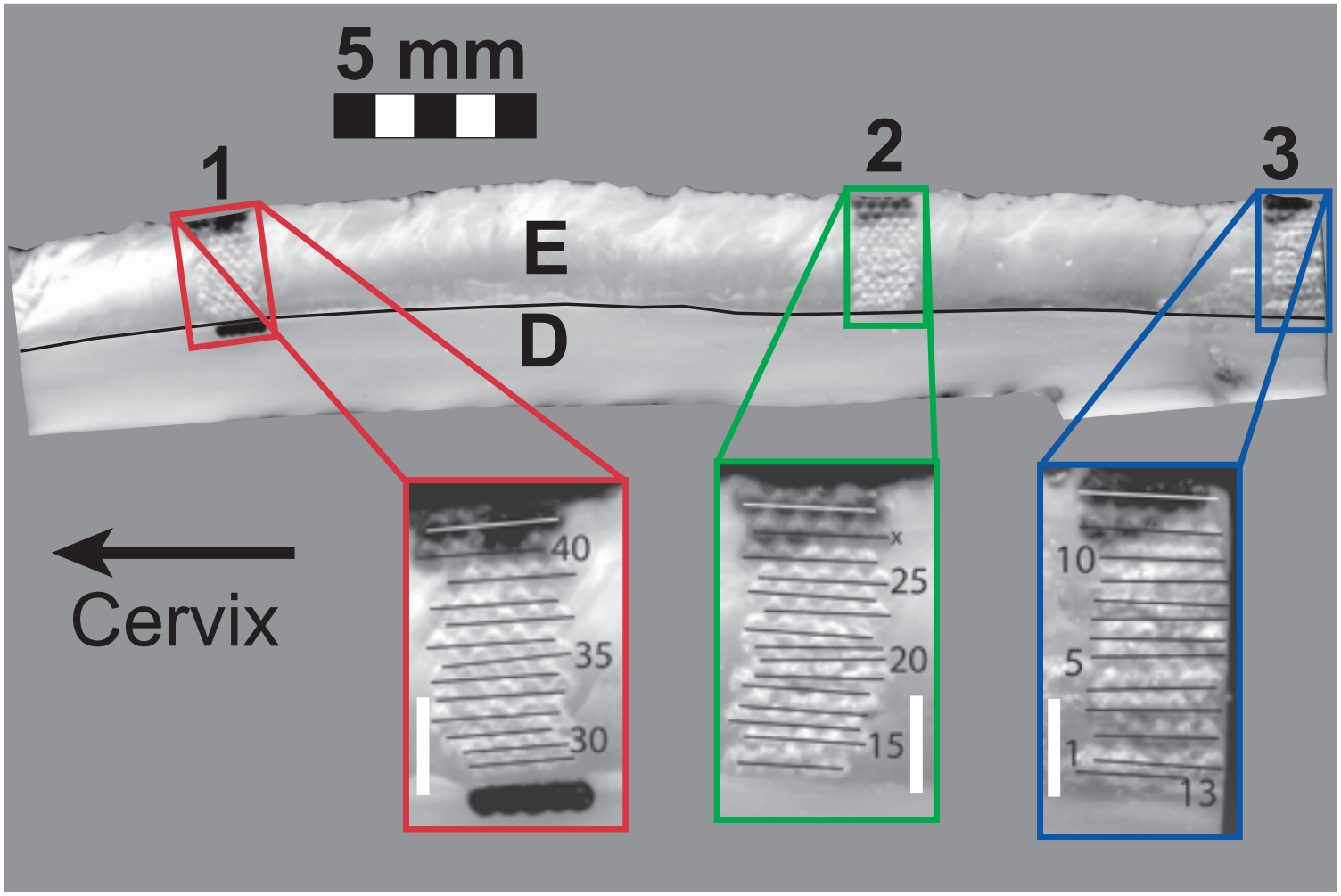

Figure S10. Image of sample Misha_Rm3.5b after sampling by LA-GC-IRMS. Profiles 1, 2, and 3, are 54, 71, and 80 mm above the cervix, respectively. The inset boxes show individual scans as black lines parallel to the EDJ. There are 5 laser pits per scan. In profile 1, one scan was done in dentin and is shown by the charred area at the base of the image. Charred scans near the outer enamel surface indicate immature enamel that contains a higher concentration of organic material than mature enamel. Width of scale bars is 5 mm in upper image and 1 mm in inset boxes.

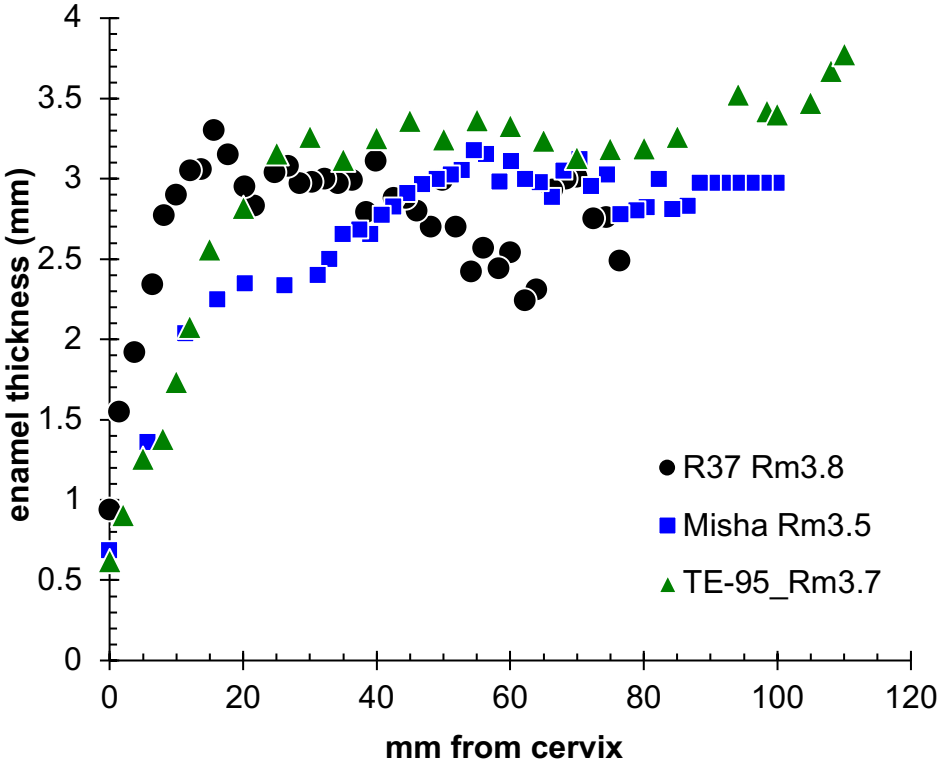

Figure S11. Enamel thickness measurements for three elephant molar plates. Misha Rm3.5 and TE-95 Rm3.7 were made on the distal side of the plate; for R37 Rm3.8, measurements were on the mesial side, which may explain differences in profile shape.

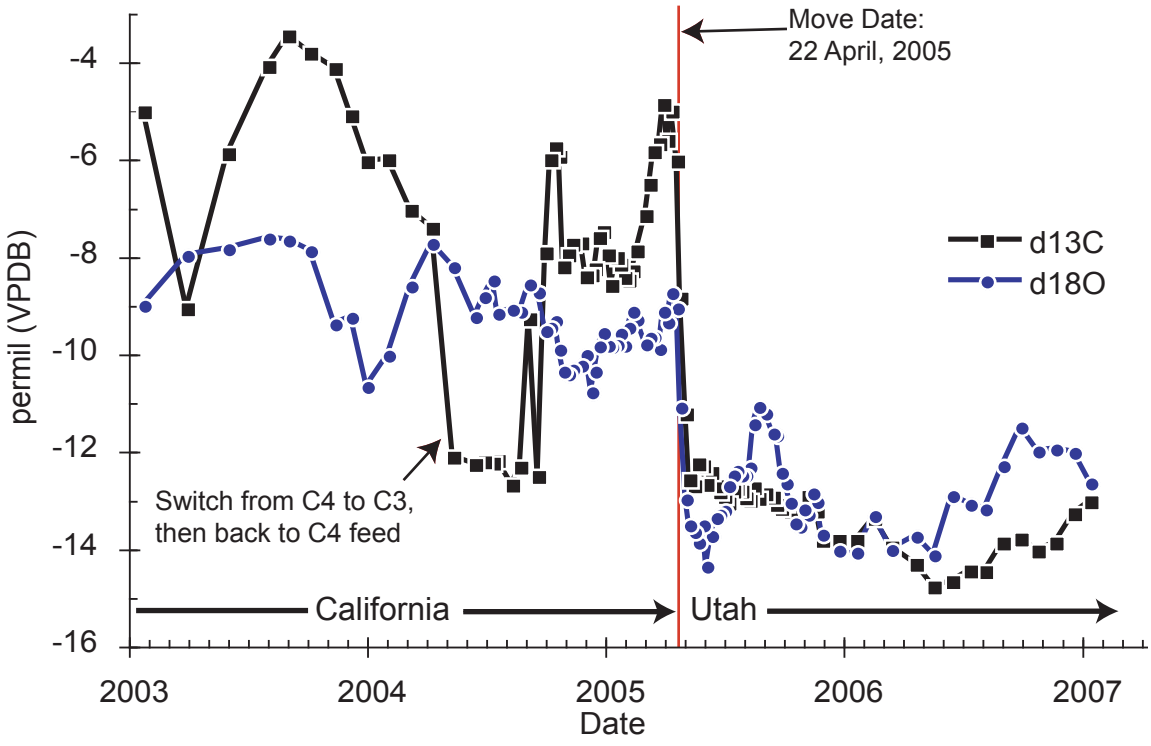

Figure S12. $\delta^{13}C$ and $\delta^{18}O$ values from Misha tusk dentin slab M640 (n=97). The time interval is from January 2003 to January 2007. The move from CA to UT occurs in late April 2005 (red line) and results in a sharp decrease in both $\delta^{13}C$ and $\delta^{18}O$ values.

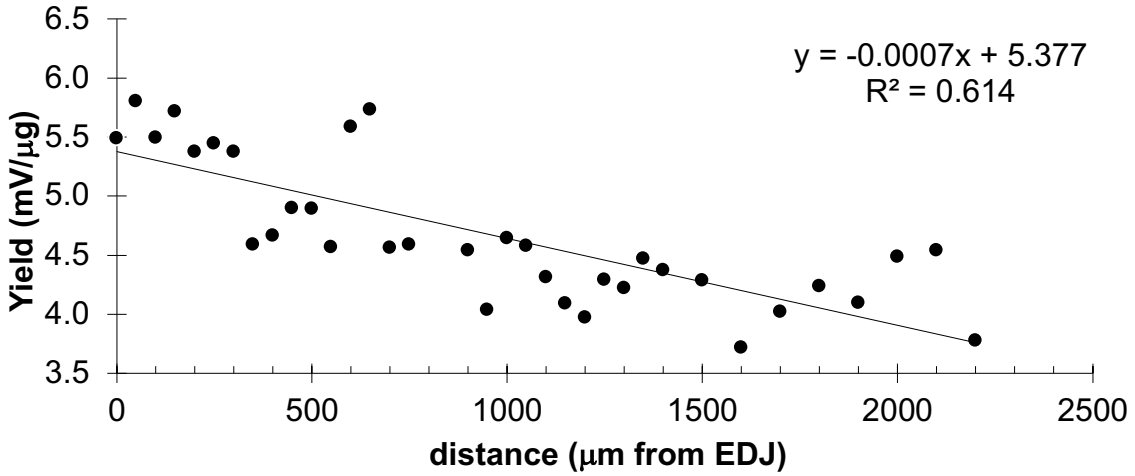

Fig S13. The decrease in CO_2 yield of micromilled samples from the EDJ to the outer enamel surface, illustrating the gradient from mature to immature enamel. The yield is determined on the mass spectrometer by millivolts per microgram of sample reacted.

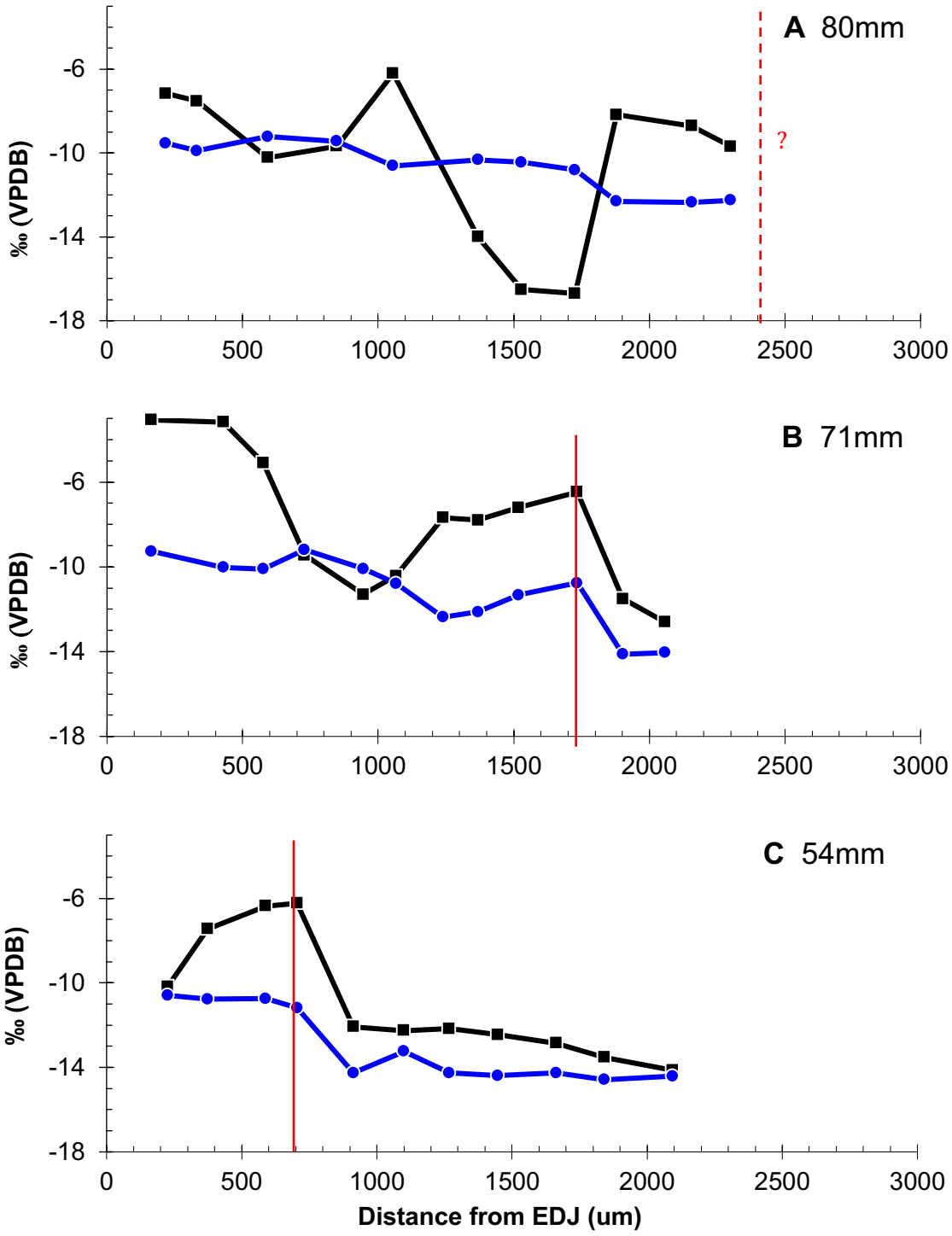

Figure S14. $\delta^{13}C$ (black squares) and $\delta^{18}O$ (blue circles) values from LA-GC-IRMS of Misha_Rm3.5b enamel. Laser scans are approximately parallel to the EDJ. The isotopic shift associated with the move from CA to UT is marked with a red line. Scan regions are 80 mm, 71 mm, 54 mm above the cervix. The shift occurs closer to the EDJ as the scan region moves closer to the cervix (A to C).

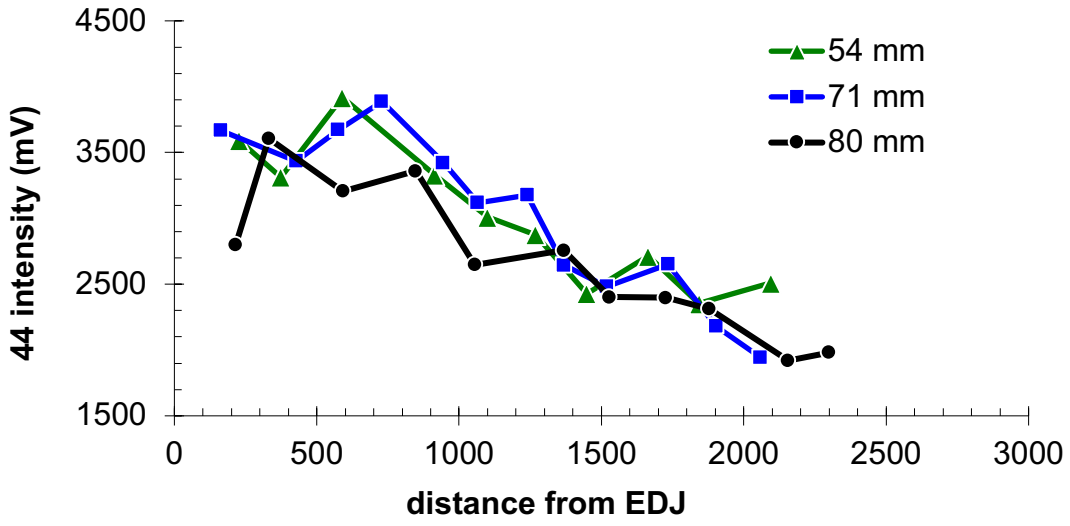

Figure S15. LA-GC-IRMS yields versus distance from the EDJ from three profiles at 54, 71, and 80 mm above the cervix. The decrease in CO_2 yield from the EDJ to the outer enamel surface suggests a linear gradient from mature to immature enamel, similar to that observed in Fig. S7B. All scans were done at the same laser settings, and yield is measured in millivolts on the major mass (44) detector of the IRMS.

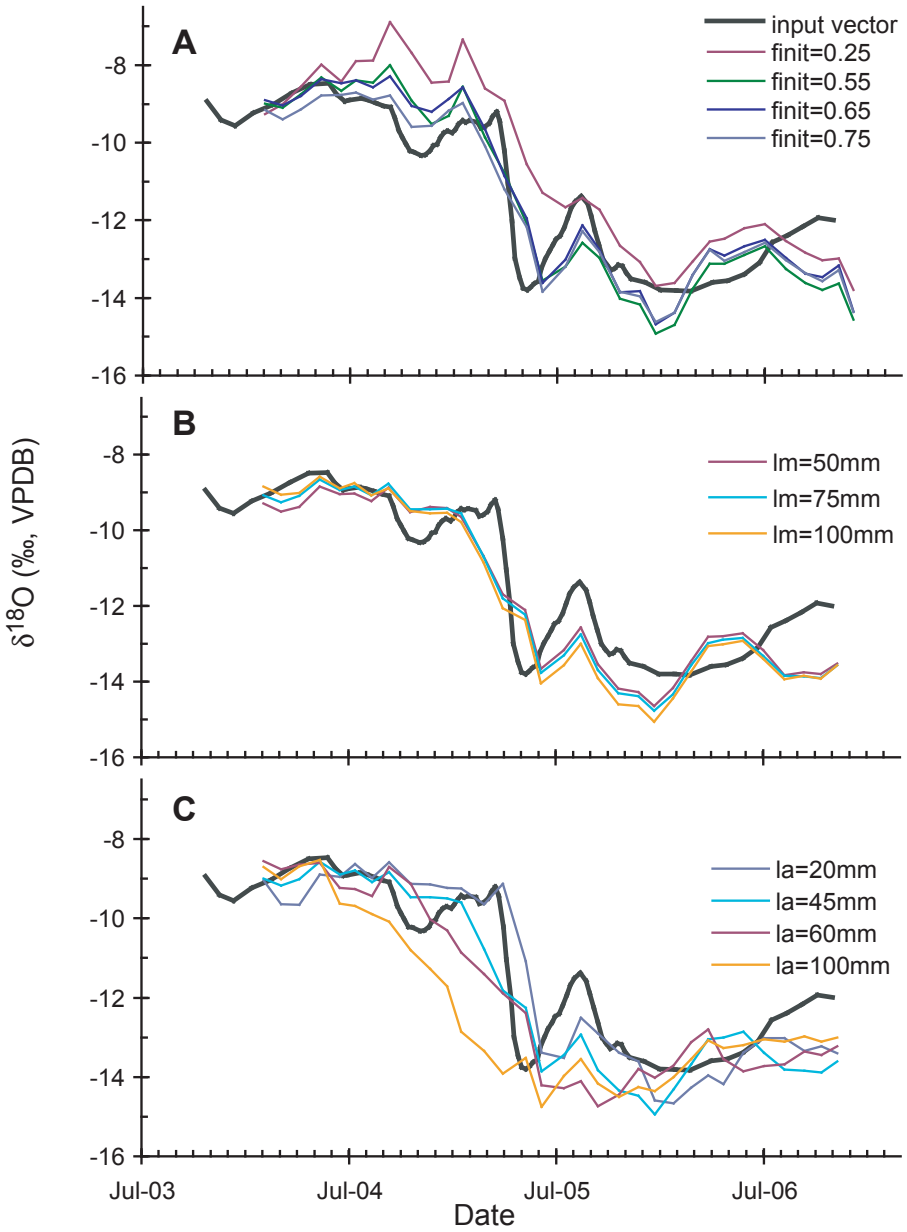

Figure S16. Sensitivity test results for A) f_i, B) l_m, and C) l_a using Misha_Rm3.5 $\delta^{18}O$ profile data. In each plot, the gray line represents the primary input signal from the M640 tusk dentin profile.